Original

Semedo, A.; Weisse, R.; Behrens, A.; Sterl, A.; Bengtsson, L.; Guenther, H.:

Projection of Global Wave Climate Change toward the End of the Twenty-First Century

In: Journal of Climate (2013) AMS

DOI: 10.1175/JCLI-D-12-00658.1

Projection of Global Wave Climate Change toward the End of the Twenty-First Century

ALVARO SEMEDO*

Department of Earth Sciences, Uppsala University, Uppsala, Sweden

RALF WEISSE AND ARNO BEHRENS

Helmholtz-Zentrum Geesthacht Centre for Materials and Coastal Research, Geesthacht, Germany

ANDREAS STERL

Royal Netherlands Meteorological Institute (KNMI), De Bilt, Netherlands

LENNART BENGTSSON

National Centre for Earth Observation, University of Reading, Reading, United Kingdom

HEINZ GÜNTHER

Helmholtz-Zentrum Geesthacht Centre for Materials and Coastal Research, Geesthacht, Germany

(Manuscript received 17 September 2012, in final form 15 February 2013)

ABSTRACT

Wind-generated waves at the sea surface are of outstanding importance for both their practical relevance in many aspects, such as coastal erosion, protection, or safety of navigation, and for their scientific relevance in modifying fluxes at the air–sea interface. So far, long-term changes in ocean wave climate have been studied mostly from a regional perspective with global dynamical studies emerging only recently. Here a global wave climate study is presented, in which a global wave model [Wave Ocean Model (WAM)] is driven by atmospheric forcing from a global climate model (ECHAM5) for present-day and potential future climate conditions represented by the Intergovernmental Panel for Climate Change (IPCC) A1B emission scenario. It is found that changes in mean and extreme wave climate toward the end of the twenty-first century are small to moderate, with the largest signals being a poleward shift in the annual mean and extreme significant wave heights in the midlatitudes of both hemispheres, more pronounced in the Southern Hemisphere and most likely associated with a corresponding shift in midlatitude storm tracks. These changes are broadly consistent with results from the few studies available so far. The projected changes in the mean wave periods, associated with the changes in the wave climate in the middle to high latitudes, are also shown, revealing a moderate increase in the equatorial eastern side of the ocean basins. This study presents a step forward toward a larger ensemble of global wave climate projections required to better assess robustness and uncertainty of potential future wave climate change.

1. Introduction

The twentieth century climate exhibited a clear warming trend, be it in the atmosphere or in the oceans. There is a broad scientific consensus that this warming is caused by the enhanced atmospheric greenhouse gases concentration, particularly carbon dioxide, due to anthropogenic emissions. The climate will continue to warm at least until the end of the twenty-first century, due to the inertia of the Earth climate system but also due to additional greenhouse gases emissions (Solomon et al. 2007). This paper deals with the impact of a warmer climate on the global wind waves climate.

Wind-generated waves (referred to simply as ''waves'' here) at the sea surface play a major role in many engineering and environmental issues, both in the open

* Additional affiliation: Escola Naval-CINAV, Lisbon, Portugal.

Corresponding author address: Alvaro Semedo, Escola Naval-CINAV, Base Naval de Lisboa, Alfeite, 2810-001 Almada, Portugal.
E-mail: alvaro.semedo@met.uu.se

DOI: 10.1175/JCLI-D-12-00658.1

ocean and coastal zones, providing a significant contribution to coastal sea level extremes and subsequent flooding. They are also a key factor in determining rates of coastal erosion and sediment budgets. At open sea, they represent a major hazard for any offshore operation or structure or to maritime transportation and shipping activity. Changes in wave climate are therefore of central importance for almost all aspects of coastal and offshore activities. From a scientific perspective, waves represent a key process, in the climate system, modifying the exchange of momentum, heat, and mass across the air–sea interface (e.g., Sullivan et al. 2008; Smedman et al. 2009; Högström et al. 2009; Semedo et al. 2009; Nilsson et al. 2012; Cavaleri et al. 2012). Changes in wave climate may change the pattern of such fluxes in a long-term perspective, and its study is therefore paramount.

Despite their outstanding relevance in the climate system, systematic approaches in studying long-term wave climate changes from a global perspective are rather limited. Analyses of recent and ongoing changes rely mostly on observations from voluntary observing ships (VOS) with known biases (e.g., Gulev et al. 2003; Gulev and Grigorieva 2004) or on global wave datasets produced within wave reanalysis (e.g., Caires et al. 2004; Sterl and Caires 2005; Caires and Sterl 2005; Caires et al. 2005; Semedo et al. 2011; Chawla et al. 2011, 2013). Satellite altimetry combined with wave model hindcasts (e.g., Young 1999; Chen et al. 2002) or only remote sensing data (Young et al. 2011) have also been used for present-day global wave climate studies. Nevertheless recent changes in the global wave climate received only minimal attention in the Intergovernmental Panel for Climate Change (IPCC) Fourth Assessment Report (AR4; Solomon et al. 2007) and were mostly based on VOS observations. Future global wave climate projections also received little attention in the IPCC AR4 and were only based on statistical projections.

The great majority of the future wave climate projections presently available in the literature were provided at regional scales (e.g., WASA Group 1998; Kaas et al. 2001, Debernhard et al. 2002; Grabemann and Weisse 2008; Debernhard and Roed 2008; Zacharioudaki et al. 2011). The intercomparison between different regional studies remains limited because of different regional domains, periods, models, and scenarios used. Most of these studies have ignored the effect of remotely generated swell, as mentioned by Lowe et al. (2009), due to the lack of global or large-scale wave climate simulations. As shown by Semedo et al. (2011), corroborating previous findings by Chen et al. (2002) and Gulev and Grigorieva (2006), the global wave field is strongly dominated by swell waves. They have also found that the wave climate variability is also dominated by changes in swell waves carrying the effect of changes in surface winds into large areas. Therefore, any conclusions on the regional wave climate projections drawn from model results that have excluded large-scale wave patterns should be used with caution (Zacharioudaki et al. 2011).

On a global scale, up until recently, future wave climate studies were only available from statistical approaches (e.g., Wang et al. 2004; Wang and Swail 2006a,b). Large-scale changes in future ocean wave climate emerging from these studies are mostly consistent with midlatitude storm tracks changes, more pronounced in the Southern Hemisphere (Wang and Swail 2006a). Compared to wave climate projections using dynamical models, statistical approaches are computationally less demanding and may be used to sample a larger range of emission and climate model uncertainties but may encounter difficulties in reproducing the observed wave field in regions where wind and waves are not in equilibrium: that is, in swell dominated zones, which are in fact predominant (Hanley et al. 2010; Semedo et al. 2011). Because of computational constraints, dynamical approaches were unavailable on a global scale up until recently. Mori et al. (2010) presented the first dynamical global wave climate projection. They ran the Simulating Waves Nearshore (SWAN) wave model (Booij et al. 1999) for three different time slices: present, near-future, and future conditions at the end of the twenty-first century. The wave model domain was of nearly global extent (80°S–80°N) using a 1.25° spatial grid size. The model was driven with near-surface marine wind fields obtained from a high-resolution (T959L60; Kitoh et al. 2009) global climate model (GCM) run under the A1B emission scenario. Apart from small-scale regional changes Mori et al. (2010) described a large-scale pattern of wave climate change that mostly resembles a poleward shift of midlatitude storm tracks, particularly in the Southern Hemisphere, broadly consistent with the results obtained from the previous statistical approaches (Wang et al. 2004; Wang and Swail 2006a,b).

The lack of coherent global ocean wave climate projections was recently acknowledged by the Coordinated Ocean Wave Climate Projection (COWCLIP) project workshop, supported by the World Climate Research Program (WCRP) and the Joint Technical Commission for Oceanography and Marine Meteorology (JCOMM) of the World Meteorological Organization (WMO) and the Intergovernmental Oceanographic Commission (IOC) of the United Nations Educational, Scientific and Cultural Organization (UNESCO). The key recommendation from this workshop was the development of an ocean wave climate community, fostering the coordination of global wave climate projections for intercomparison

between international research groups, to understand uncertainties within the community ensemble (Hemer et al. 2012).

Bengtsson et al. (2009) carried out a time-slice climate projection experiment using a high-resolution (T213, 63km) configuration of the Max Plank Institute (MPI) ECHAM5 atmosphere GCM (Roeckner et al. 2003), for two 32-yr periods (at the end of the twentieth and twenty-first centuries) for the IPCC A1B scenario. Their goal was to assess the changes in the track, intensity, and frequency of extratropical storms in a warmer climate. They have concluded that the high resolution of the experiment allowed for better resolved extratropical storms, and their main findings were that in a warmer climate extratropical cyclones will not necessarily get more intense but a poleward shift of the storm tracks, particularly in the Southern Hemisphere, is to be expected, with corresponding changes in the surface marine winds pattern.

The investigation of the effect of these changes on the late twenty-first century global wave climate is the main goal of the present study. The ECHAM5 near-surface winds are used to force the Wave Ocean Model (WAM; WAMDI Group 1988) in both periods. The twentieth-century period will be referred to as the control run. The wave fields from the control run are compared to the 40-yr European Centre for Medium-Range Weather Forecasts (ECMWF) Re-Analysis (ERA-40; Uppala et al. 2005; Sterl and Caires 2005) and Interim ECMWF Re-Analysis (ERA-Interim; Dee et al. 2011) wave reanalyses and validated against long-term quality controlled in situ buoy wave height observations. The dynamically based global wave climate projections in this study are part of the COWCLIP ensemble effort (Hemer et al. 2013).

The paper continues in section 2, where the wave model, the experiment, and the wave and atmospheric data used here are briefly described. Subsequently, in section 3 the results of the control run wave model integration are compared and validated against reanalyzes and observations for present-day conditions. The results of the climate change experiment are presented in section 4. In section 5, the results are summarized and the concluding remarks along with suggestions for further research are presented.

2. Models, data, and experiment

a. Atmospheric climate data

The wave model integrations in the present study were driven with near-surface marine wind fields at 10-m height U_{10}. These U_{10} winds were derived from the global time-slice climate simulation of Bengtsson et al. (2009), where a T213 version of the MPI ECHAM5 atmosphere GCM was used, corresponding to a spatial horizontal grid resolution of about 63 km (with 31 vertical levels). The experiment was based on the IPCC A1B greenhouse gas emission scenario, which is usually referred to as a ''medium–high emissions'' scenario. The GCM was used to simulate the climate of two 32-yr periods, representative of the end of the twentieth (1959–90) and twenty-first (1969–2100) centuries. Comparisons of the present climate run with observations and reanalysis (ERA-40 and ERA-Interim) showed the capability of the ECHAM5 model T213 runs to produce realistic results, particularly of the properties of the extratropical cyclones, both qualitatively and quantitatively, with considerable gains due to the increased resolution (Bengtsson et al. 2009). The experiments and their results in terms of windstorm statistics, as well as additional details on the ECHAM5 setup, are described in detail in Bengtsson et al. (2006, 2007, 2009).

The near-surface marine wind fields were provided by the GCM every 6 h; for driving the wave model these wind fields were bilinearly interpolated in space to match the wave model grid (see below) and they were kept constant in time over a period of 6 h until the next wind field from the climate model was available. Additionally, sea ice conditions obtained from the same ECHAM5 simulations were provided to the wave model and updated every 24 h.

b. Wave model

The ocean wave model WAM cycle 4.5.3 is used in this study. WAM cycle 4.5.3 is an update of the WAM cycle 4 wave model described in Komen et al. (1994) and Günther et al. (1992). In WAM cycle 4.5.3 the basic parameterizations and numerical schemes of WAM cycle 4 are kept, but the source function integration scheme developed by Hersbach and Janssen (1999) and the model updates described in Bidlot et al. (2007) are incorporated. Other major changes introduced in the model update are mostly of technical nature. The wave model experiments described below were performed on a regular nearly global latitude–longitude grid, covering a latitude range of 78°S–80°N and using a fixed spatial grid size of 0.5°. The spectral domain was discretized into 25 logarithmically spaced frequency bins, ranging from 0.041 to 0.411 Hz, corresponding to wavelengths of about 10–950 m. Wave propagating directions were represented using a resolution of 15°. The model was run in shallow water mode, taking shoaling and wave energy dissipation at the sea floor into account. The 1-minute gridded elevations/bathymetry for the world (ETOPO1) bathymetry data (NGDC 2010), at 1-min (~0.016°) resolution, was used.

The wave model experiments were performed using integration time steps of 5 and 10 min, for the advection

and the source functions, respectively. For the whole experiment the wave spectra obtained at each model grid point were stored every 6 h. These spectra were stored mainly for use as boundary conditions for future regional wave climate projection studies. Additionally, 29 wave parameters derived from different forms of integrating the wave spectra were stored (see Table A1 in the appendix). The wave model was integrated for the same time slices as the ECHAM5 experiment periods mentioned above. The twentieth-century 1959–90 period, representative of present-day conditions, serves as the control run against which late-twenty-first-century (2069–2100) future changes in wave climate are assessed. The twentieth- and the twenty-first-century future climate projections will hereafter be mentioned for convenience as PC20 and FC21, respectively.

c. *Validation data: Reanalyses and buoy data*

The wave model capability to represent the present wave climate is assessed by comparing the PC20 against the ECMWF ERA-40 and ERA-Interim wave reanalyses. Both ERA-40 and ERA-Interim are reanalyses of meteorological observations, with the former covering the period from September 1957 to August 2002 (here we use only the period from 1958 to 2001) and the latter covering the period from 1 January 1979 onward and continuing to be extended in near–real time (here we use the period from 1979 to 2011). Besides atmospheric variables, both reanalyses also include wave parameters, generated by a two-way coupled atmosphere–wave model systems, where wind fields and other atmospheric parameters that influence wave growth are passed to the wave model, which returns information about the impact of the sea state on surface roughness via the Charnok parameter (Janssen 1991, 2004). The wave model used in both coupled model systems was also the WAM model.

ERA-40 is a second-generation reanalysis and the first to use a two-way coupled atmosphere–wave model system, with a three-dimensional variational data assimilation (3DVAR) scheme. The ERA-40 wave data consist of 6-hourly global fields with a 1.5° × 1.5° grid resolution. Sterl and Caires (2005) produced a statistically corrected dataset of the ERA-40 significant wave height H_s (CERA-40). The PC20 H_s global fields are compared to the CERA-40. Additional details about ERA-40 wave reanalysis are given by Sterl and Caires (2005), Caires and Sterl (2005), and Caires et al. (2005). Details about comparisons of the ERA-40 against similar reanalysis products are given by Caires et al. (2004).

ERA-Interim is the most recent ECMWF reanalysis. It is based on a slightly different atmospheric model than the one used in ERA-40 and uses a two-way coupled atmosphere–wave model system as well. It also consists of 6-hourly global fields with a 1° × 1° grid resolution. The wave model WAM also received some improvements, including a revised formulation of the ocean wave dissipation scheme, and the introduction of a new scheme to parameterize unresolved bathymetry (Bidlot et al. 2007). A four-dimensional variational data assimilation (4DVAR) scheme was used in ERA-Interim. The two-dimensional spectra include 30 wave frequencies and 24 direction bins (higher than ERA-40: 25 frequencies and 12 directions). The PC20 H_s and the ECHAM5 U_{10} winds (just wind speed) global fields are compared to the equivalent ERA-Interim parameters. Additional details about the ERA-Interim reanalyses are given by Dee and Uppala (2009) and Dee et al. (2011).

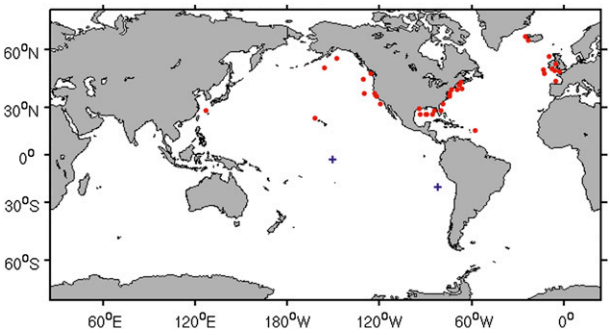

FIG. 1. Buoy position. The red dots represent the Northern Hemisphere buoys, and the blue crosses represent the two Southern Hemisphere buoys.

The PC20 H_s are also validated against more than 50 in situ buoy and platform wave observations. These data were quality controlled at the ECMWF, as part of the ongoing verification of the forecasting performance of operational wave models with buoy data (Bidlot et al. 2002). From all the buoy data available since 1979 only buoys positioned in relatively deep waters were selected, and from these only the ones with at least a 10-yr-long time series. The exceptions were the only two buoys in the Southern Hemisphere, which have 9- and 8-yr-long records. The buoy data were time averaged and collocated with PC20 data following the same procedure as in Bidlot et al. (2002). Figure 1 shows the position of the buoys used in the validation (see Table A2 in the appendix for further details on the buoys).

In the PC20 and ECHAM5 comparisons with the reanalyses and validation against buoy observations the time constraint is ignored. Since the ECHAM5 integration and the wave model WAM runs were not subject to data assimilation, they are considered as representative of the present-day climatological mean atmospheric and wave climates, respectively, regardless of the time period. Hence, the comparisons were made between the

PC20/ECHAM5 (1979–90) and the CERA-40 (1958–2001) and the ERA-Interim (1979–2010) reanalyses. The same applies for the buoy validation, whereas in this case the buoy time series length is shorter.

3. Validation of the wave climate in the reference period

The normalized differences between the long-term averages of the annual mean H_s and of the annual mean H_s 95% percentile, derived from PC20 and CERA-40 and from PC20 and ERA-Interim (PC20 minus reanalysis normalized by the reanalysis), are shown in Figs. 2a–d. In most extratropical areas the PC20 mean H_s values are within 5%–15% (20–25 cm) of CERA-40 (Fig. 2a). In the North Atlantic the differences between PC20 and CERA-40 are lower (less than 5%; ~15 cm), and in the tropics, especially in the Pacific Ocean, they are higher (around 25%–30% and higher than that along the equator and the west coast of Central America). The seasonal differences [for December–February (DJF) and June—August (JJA); not shown] are of the same order of magnitude, although less pronounced in the equatorial areas in the boreal winter. This fact is most probably due to the lower swell significant wave heights in the lower latitudes in JJA (Semedo et al. 2011) and to the northward migration of the swell front (Young 1999; Semedo et al. 2011), particularly in the Pacific Ocean.

The annual mean 95% percentile H_s values of PC20 are also higher than the CERA-40 ones (Fig. 2b). The highest differences are not only confined to the low and tropical latitudes but are also present in the midlatitudes of the North Pacific subbasin. The CERA-40 H_s fields are a statistically corrected product (with in situ buoy observations), but, on the other hand, this reanalysis is known to underforecast extreme waves, most probably due to an underforecast of high surface wind speeds (P. Janssen 2004, personal communication; as in Sterl and Caires 2005). Although that might be an explanation for the differences found between PC20 and CERA-40, the first conclusion to be drawn is that the former probably overforecasts wave heights, particularly in the low latitudes.

Figures 2c,d show the differences between the annual PC20 means and the annual ERA-Interim means of the H_s and the H_s 95% percentiles. The difference patterns are similar to those for CERA-40 but have smaller amplitudes in the low and tropical latitudes, particularly in the Atlantic Ocean. In the Pacific Ocean, also in the low and tropical latitudes, the behavior of PC20 is similar, although showing lower differences along the coast of Central America. Recent analysis has shown that ERA-Interim compares better with buoy and remote sensing

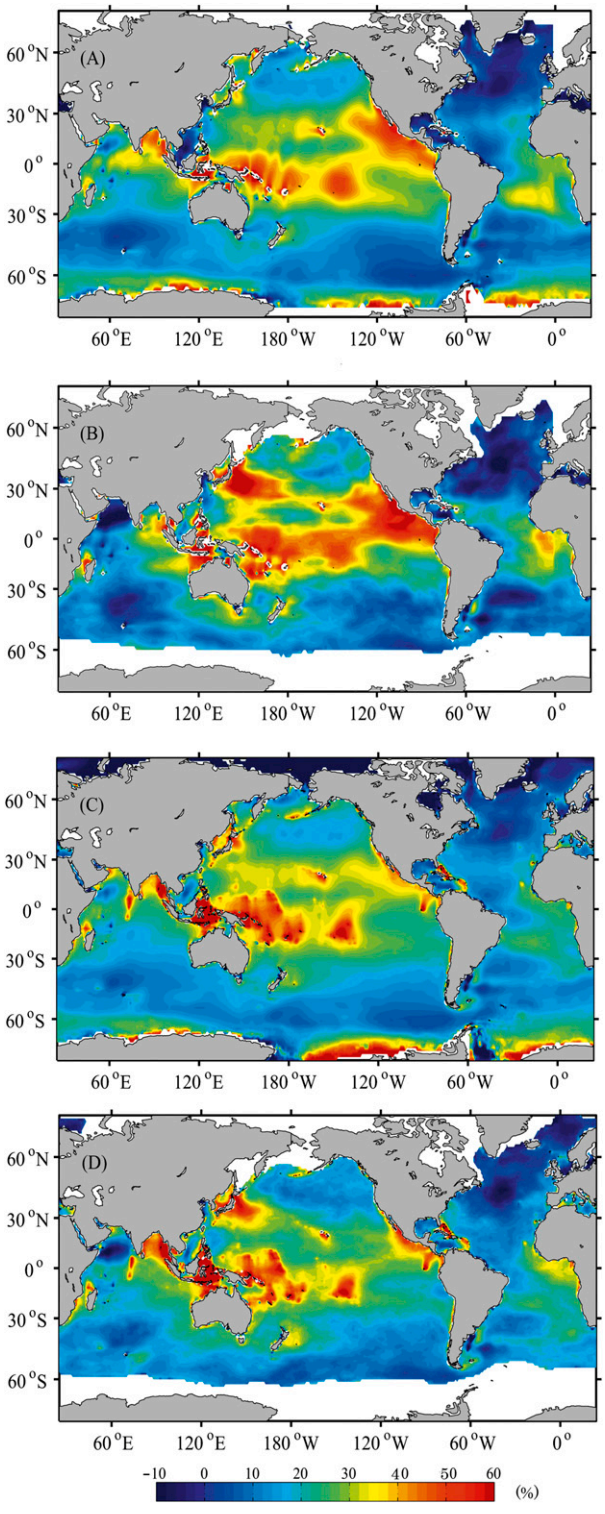

FIG. 2. Normalized differences (in %) between the annual H_s means and the annual H_s 95% percentile means (a),(b) of PC20 and CERA-40 and (c),(d) of PC20 and ERA-Interim. PC20 minus reanalysis is normalized by the reanalysis.

observations than the statistically corrected CERA-40 (J. Bidlot 2012, personal communication). The reasons are, most probably, better reanalyzed U_{10} winds but also the improvements in the WAM model (Bidlot et al. 2007; Dee et al. 2011; Bidlot 2012). The DJF and JJA differences (not shown) between the PC20 and the ERA-Interim H_s and 95% percentiles are similar to the ones with CERA-40 but, in line with the annual differences, less pronounced.

The normalized differences between the long-term averages of the annual mean wave period T_{m1} from PC20 and ERA-Interim were also computed (not shown). The mean periods used here are the mean periods from the first moment (for further details, see Bidlot 2001; Semedo et al. 2011). As for H_s the PC20 has a tendency to overestimate the mean wave T_{m1}, more in the Southern Hemisphere. These differences are less than 7%, with exception of the North Atlantic and southern Indian trade winds, where the differences can be higher than 10%.

Figures 3a,b show the differences between the annual means of the ECHAM5 and ERA-Interim U_{10} and U_{10} 95% percentile. The color scale in Fig. 3 is different than the one used in Fig. 2, and can also vary between subsequent figures below. Since CERA-40 has only H_s fields, this comparison was only done for ERA-Interim. As can be seen, the differences between PC20 and ERA-Interim U_{10} annual means (Fig. 3a) lie mostly between −10% and 20%, being positive, in 78% of the global ocean. The PC20 near-surface wind speeds are lower than the ERA-Interim ones along the equator in all ocean basins, particularly in the Atlantic Ocean. The differences in the middle to high latitudes are smaller (usually 0%–5%) and higher (~10% or less) along the trade winds. The difference for the U_{10} 95% percentiles are similar, but with higher amplitudes in the western area of the Pacific Ocean and in the Southern Ocean. The patterns of the DJF and JJA seasonal differences (not shown) for both mean U_{10} and mean U_{10} 95% percentiles are not much different.

Figure 4 displays the magnitude of the H_s interannual variability bias of PC20 in relation to ERA-Interim, by comparing the variances of the yearly mean values of PC20 (σ^2_{PC}) and ERA-Interim (σ^2_{ER}). A binary logarithm was applied to the dimensionless ratio $r = \sigma^2_{\mathrm{PC}}/\sigma^2_{\mathrm{ER}}$ because of the large range of values. The magnitude of the H_s PC20 variance, while spatially variable, has a global mean comparable to ERA-Interim [when $\log_2(r) \approx 0 \rightarrow r \approx 1$] in most of the global ocean. The variance is underestimated where $\log_2(r) < 0$ and overestimated where $\log_2(r) > 0$]. The variability bias of the PC20 H_s annual field shows an adequate representation of the interannual cycle, with values of the magnitude of interannual variance

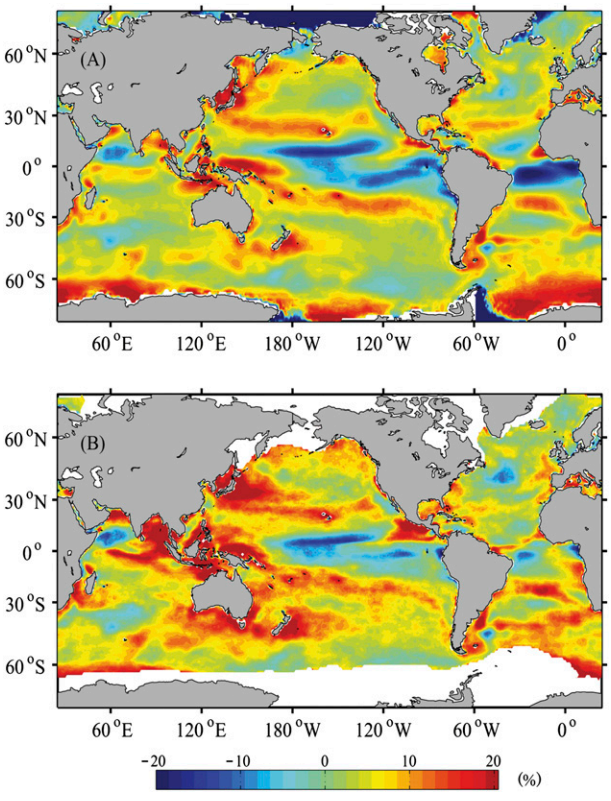

FIG. 3. Normalized differences (in %) between (a) the annual U_{10} means and (b) the annual U_{10} 95% percentile means of PC20 and ERA-Interim. PC20 minus reanalysis is normalized by the reanalysis.

of PC20 close or of the same order of magnitude of ERA-Interim.

Figure 5 shows the time series of the globally averaged CERA-40, ERA-Interim, and PC20 yearly mean H_s, normalized by their mean value. The yearly means are computed between 75°N and 75°S, and a latitudinal correction is applied (cosine of the latitude). These time series are presented here to give a synthesized picture of the interannual variability of the three datasets and of how the PC20 long-term H_s trend compares with the two reanalysis. In terms of long-term trend the PC20 behavior does not show any particular disagreement with the two reanalyses. In 1975, CERA-40 shows a pronounced deep, already noted by Sterl and Caires (2005), whereas in the PC20 simulation does not show such large variations during the all run. During the period when the three datasets overlap (1979–90), the agreement between them in terms of trends is clear.

The results of the validation of the PC20 mean H_s annual values against long-term buoy observations are shown in Figs. 6a,b. The scatterplot in Fig. 6a compares the H_s buoy observations with the PC20 H_s values and

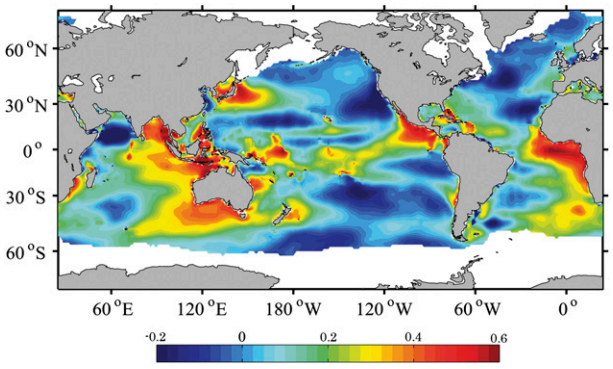

FIG. 4. Variability bias (dimensionless) between the PC20 and ERA-Interim yearly variances: $\log_2(\sigma^2_{PC}/\sigma^2_{ER})$.

with the H_s ERA-Interim values. A generalized overestimation of PC20 is present in the highest waves (on the order of 10–20 cm), with an overall root-mean-square difference (RMSD) of 0.39 m and a positive bias of 0.16 m, while the reanalysis RMSD is 0.16 m and has a slightly negative bias of −0.02 m. For lower H_s values the overestimation is lower but still present. On the other hand, ERA-Interim slightly underestimates the observed H_s values, although it is more coherent and closer to the observations. The probability density functions (pdf) of the buoy observations, and the PC20 and the ERA-Interim H_s values are shown in Fig. 6b. The pdf profiles are rather similar, with the exceptions being the underestimation of both PC20 and ERA-Interim in the lower (~1 m) H_s values and the overestimation of PC20 for the highest waves, confirming what was shown in the scatterplot.

The validation and comparison of the PC20 H_s against observations and reanalyses, respectively, showed that the control run has a tendency to overforecast wave heights. This is more pronounced in some areas, like in the lower latitudes of the Pacific Ocean and in the Southern Ocean. In the lower latitudes, where swell waves prevail, particularly in the eastern areas of the ocean basins (Young 1999; Semedo et al. 2011), the climatological mean wave heights are low compared to higher latitudes. There, in spite of the large H_s differences in percentage, the magnitude of the differences is relatively small when compared to middle or high latitudes, where extratropical storms and strong winds prevail and the mean H_s values are substantially higher. These higher PC20 H_s values in the lower latitudes can be explained by the overforecast of the control run along the Southern Ocean (less than 10% compared to the reanalyses; see Fig. 2), with these waves propagating northward as swell and contributing to higher waves between ~20°N and 20°S.

The agreement between the control run PC20 H_s and the reanalyzes and the buoy observations shows that the WAM model, forced by the ECHAM5 U_{10} winds, produces realistic results of the global wave climate at end of the twentieth century. These results follow from the good agreement of the ECHAM5 U_{10} winds, already noted by Bengtsson et al. (2009). This gives us the confidence in the ability of the model to simulate a realistic climate change signal.

4. Climate and climate change signals

a. Climate of the reference period

The long-term climatological annual mean H_s for present-day conditions shows pronounced maxima in the midlatitudes of both hemispheres associated with the midlatitude storm tracks (Fig. 7a). The wave heights are highest in the Indian sector of the Southern Ocean, southwest of Australia, where the climatological annual mean maxima reaches values higher than 5 m. Wave heights are, on average, lower in the tropical and subtropical regions and in sheltered fetch limited areas, such as the South China Sea and the Indonesian Archipelago, the Mediterranean and the Baltic Seas, or the Gulf of Mexico. From a seasonal perspective (not shown), averaged wave heights are higher in the midlatitudes during

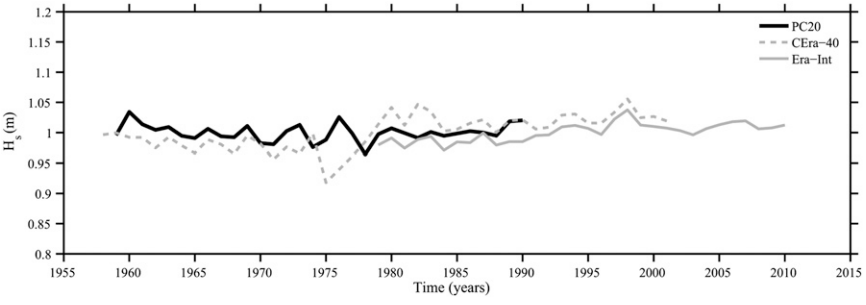

FIG. 5. Time series of the yearly mean globally averaged H_s (m) for ERA-Interim (full gray line), CERA-40 (dashed gray line), and PC20 (full black line), normalized by their mean value.

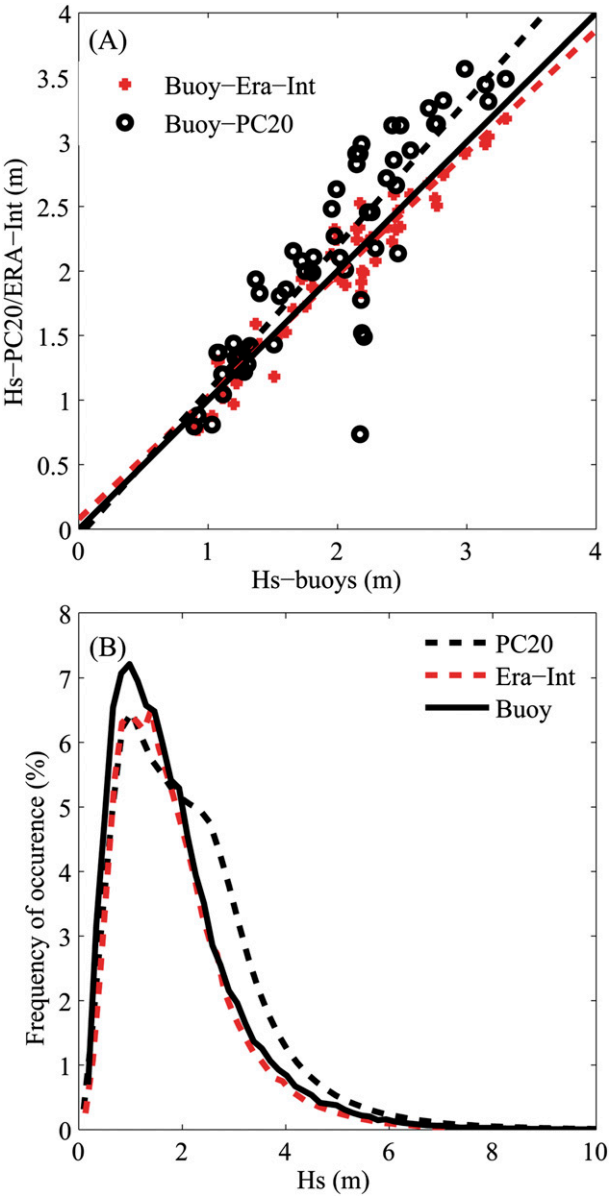

FIG. 6. Scatterplots of (a) H_s (m) for PC20 (black circles) and ERA-Interim (red crosses) against buoys observations and (b) H_s (m) pdf from buoy observations (dashed black line), PC20 (full line), and ERA-Interim (dashed red line).

the respective winter season in each hemisphere, with the Northern Hemisphere displaying a higher seasonal amplitude compared to the Southern Hemisphere. The mean H_s 95% percentile spatial pattern (not shown) is similar to the annual mean H_s one, showing mean extreme values at the climatological maxima in the midlatitude storm tracks in both hemispheres exceeding 6 m. But waves propagate away from their generation areas as swell, crossing entire ocean basins throughout thousands of kilometers (Alves 2006) along great circle paths. Therefore, the waves in the open ocean are always composed of locally generated waves and waves that were generated elsewhere and propagated as swell (Semedo et al. 2011).

The global wave height field resembles the global wind climatology. On average, near-surface marine wind speeds and their extremes are most pronounced in the midlatitudes with a seasonal climatological maxima occurring during the winter in each hemisphere (not shown). Although there is a connection between the climatological changes in the wind speed and the changes in the ocean surface waves, that connection is not necessarily direct due to the propagating effect of waves. For that reason, changes in the extratropical storms in the midlatitudes, in terms of wind speed and wind direction, will affect the wave climate, for example, in the low latitudes, where the wind climate does not necessarily show any changes.

The energy carried by waves at the ocean surface is a function of wave periods and wave heights, to the first and second order, respectively (see, e.g., Semedo et al. 2011). As waves propagate away from their generation area as swell, their height decreases and their period increases. Therefore, the climatological maxima of the mean wave periods and mean wave heights maxima do not coincide. Wave periods are climatologically longer in swell dominated regions in the low to tropical latitudes in the eastern side of the ocean basins (the so-called swell pools; Chen et al. 2002; Semedo et al. 2011).

b. *Changes in wind and wave climate toward the end of the twenty-first century*

The annual mean H_s for the present day (PC20), and the normalized difference between future and present climates (FC21 minus PC20 normalized by PC20) can be seen in Figs. 7a,b. The significance of the projected future changes (at 95% significant level) is assessed using a standard t test for difference in means. The projected changes of the global annual H_s climate, due to global warming, as reproduced by the IPCC A1B scenario, show a well-defined statistically significant increase of the wave heights in the Southern Ocean in the middle to high latitudes (poleward from around 40°S) covering the whole Southern Ocean storm belt. This increase, higher than 10%, is more pronounced in the Pacific and Atlantic sectors of the Southern Ocean (~15%), with increases of absolute annual mean H_s on the order of 0.6–0.7 m. Closer to the Antarctic coasts the increase in the mean H_s is more pronounced, particularly in the Weddell and Ross Seas. This can be explained by the retraction of the sea ice, so that in FC21, in these seas, there will be waves where in PC20 there was ice. The same applies to the Northern Hemisphere, in the east coast of Greenland

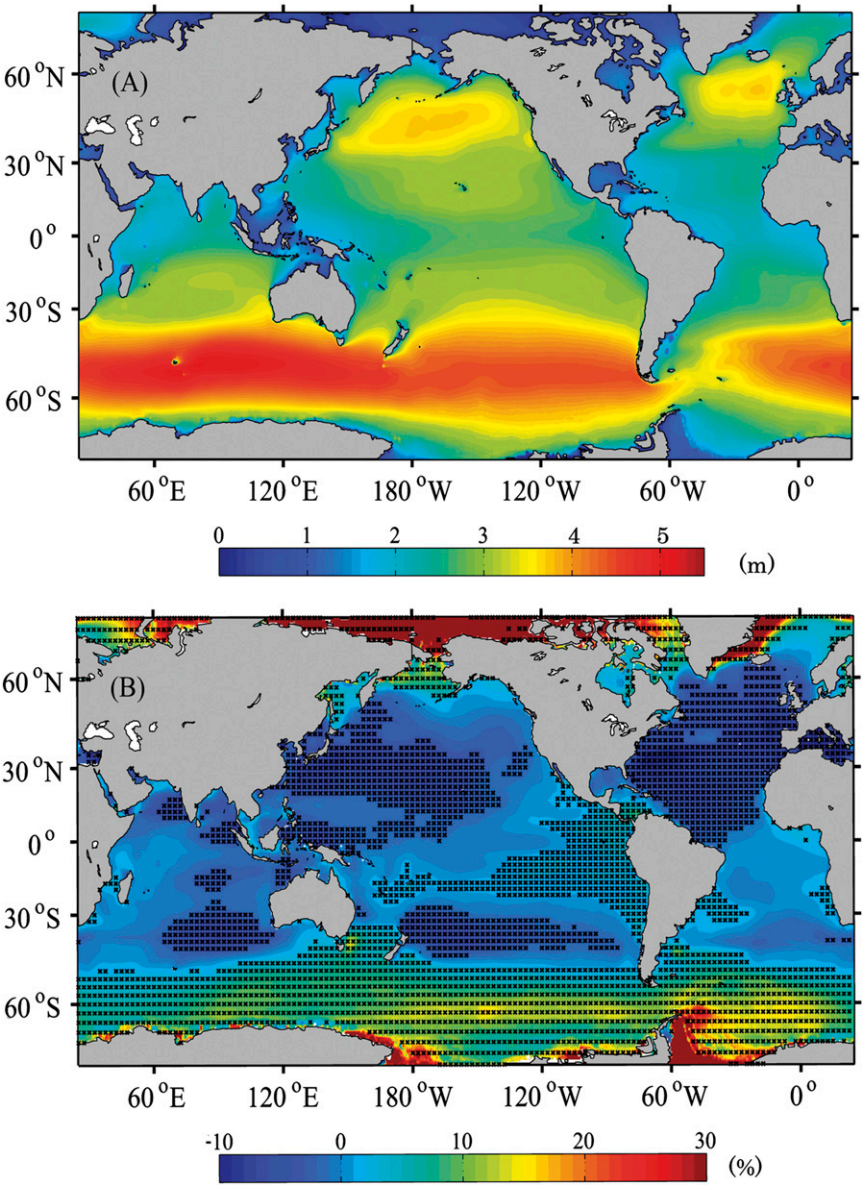

FIG. 7. (a) PC20 H_s (m) annual mean and (b) projected changes for the 2069–2100 annual mean H_s (m): FC21 minus PC20 normalized by PC20 (in %). Regions where the projected changes are statistically significant (at 95% confidence level) are marked with dots.

and at the Chukchi Sea, and in the Arctic Ocean. In the high latitudes of the Northern Hemisphere, there is also a statistically significant increase (close to 10%) in the annual mean H_s, in the North Atlantic, in the Norwegian Sea, and in the Bering Sea, in the North Pacific. These increases are accompanied by a generalized decrease in the wave heights in the Northern Hemisphere low and middle latitudes, particularly in the North Atlantic subbasin (more than minus 10%) off the U.S. East Coast. Along the swell pools, in the Pacific and Atlantic Oceans, a small statistically significant projected increase of the wave heights (less than 10%, corresponding to an increase on the order of 0.12 m) can also be found.

The present-day (PC20) seasonal (DJF and JJA) mean H_s for and the correspondent normalized differences are shown in Figs. 8a–d. In the boreal winter (Fig. 8b) there is a general decrease in the projected future wave heights. This decrease is more pronounced in the North Pacific subbasin (more than minus 10%), in an area extending from the east coast of Japan to the midlatitude central subbasin. A statistically significance projected increase in the wave heights can nevertheless be found in the higher

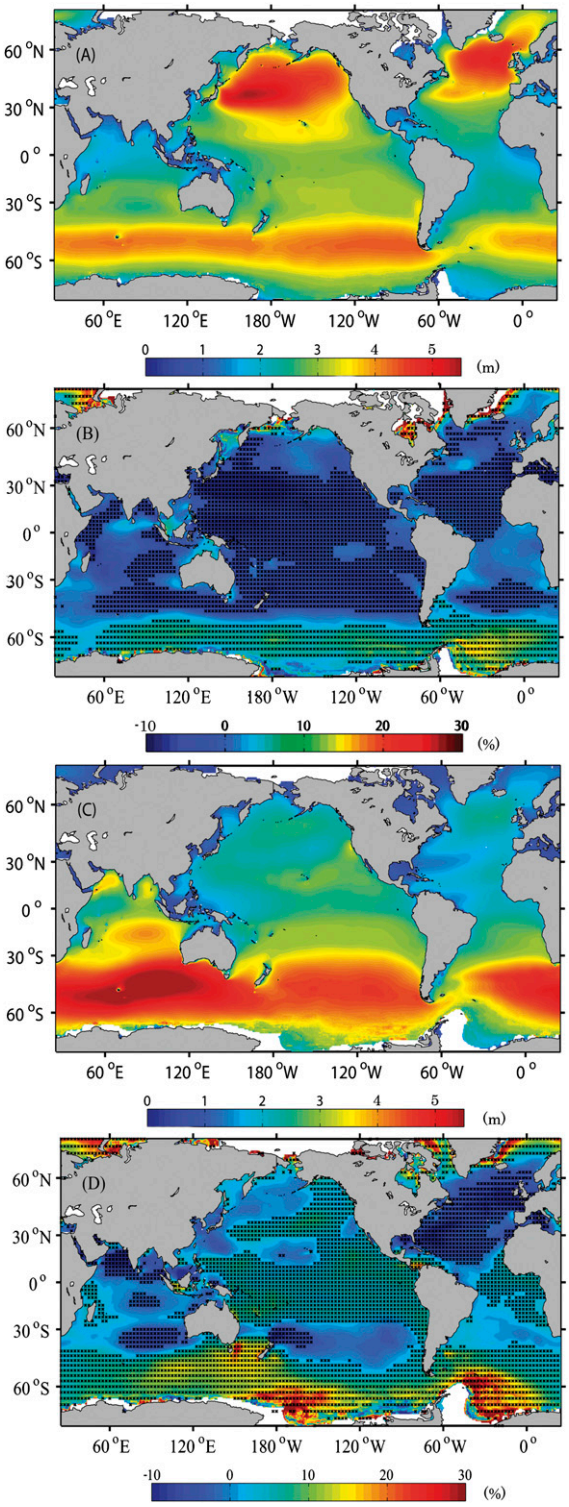

FIG. 8. PC20 H_s (m) (a) DJF and (c) JJA means and (b) DJF and (d) JJA seasonal projected changes for the 2069–2100 annual mean H_s (m): FC21 minus PC20 normalized by PC20 (in %). Regions where the projected changes are statistically significant (at 95% confidence level) are marked with dots.

latitudes of both hemispheres. This increase is more pronounced (i.e., covering a larger area) in the Southern Hemisphere, particularly in the Atlantic sector of the Southern Ocean, east of the Antarctic Peninsula (higher than 10%). For JJA (Fig. 8d) wave heights are still projected to decrease in the North Atlantic subbasin (more than minus 10%) and in a band between 30° and 50°S in the Indian and Pacific Oceans. In most of the Pacific Ocean and South Atlantic subbasin wave heights are projected to increase. Wave heights are also projected to increase in the mid to high latitudes of the Southern Hemisphere (10%–15% and close to 20% in some areas). Around Antarctica strong increases, up to 30%, are found, which are partially be related to the vanishing sea ice cover, as mentioned above.

Figures 9a–i show the north–south cross sections of the zonally averaged annual and seasonal mean H_s fields in each ocean basin. For convenience, the Southern Ocean sectors are considered as part of the respective Indian, Pacific, and Atlantic Oceans. This figure shows the poleward shift of the climatological mean H_s maxima in the midlatitudes in both hemispheres that is projected to occur at the end of the twenty-first century. In this figure, it is also possible to evaluate the increase or decrease of the future annual and seasonal mean wave heights with latitude, compared to the present time H_s climate. In the Southern Hemisphere the poleward shift of the projected future annual and seasonal H_s maxima is clearly visible in the three ocean basins, in line with the results from Figs. 7b and 8b,d. Along with the poleward shift, the mean wave heights in the midlatitudes in the Southern Hemisphere also increase in FC21 in all oceans, particularly in JJA in the Indian Ocean, with an increase of more than 0.5 m. In the Northern Hemisphere midlatitudes the situation is more complex. There is poleward shift at the annual mean climatological H_s maxima in the North Pacific and a slight decrease of annual and DJF wave heights at the climatological maxima. In the North Atlantic subbasin, the decrease of the annual and seasonal mean wave heights maxima is more pronounced, practically without any latitudinal shift. At higher latitudes, an increase in the wave heights is projected to occur. In the tropical and low latitudes the latitudinal variation of the mean H_s is small or negligible in the annual fields, with the exception of a slight decrease in the wave heights between 15° and 45°N in the North Pacific and North Atlantic subbasins. That is not the case in DJF, where the projected future mean wave heights decrease, particularly in the Pacific Ocean. In JJA, on the other hand, a slight increase is to be expected.

Quantile–quantile (Q-Q) plots, comparing the present and future percentiles of the annual and seasonal wave heights, are shown in Figs. 10a–i. The annual and seasonal

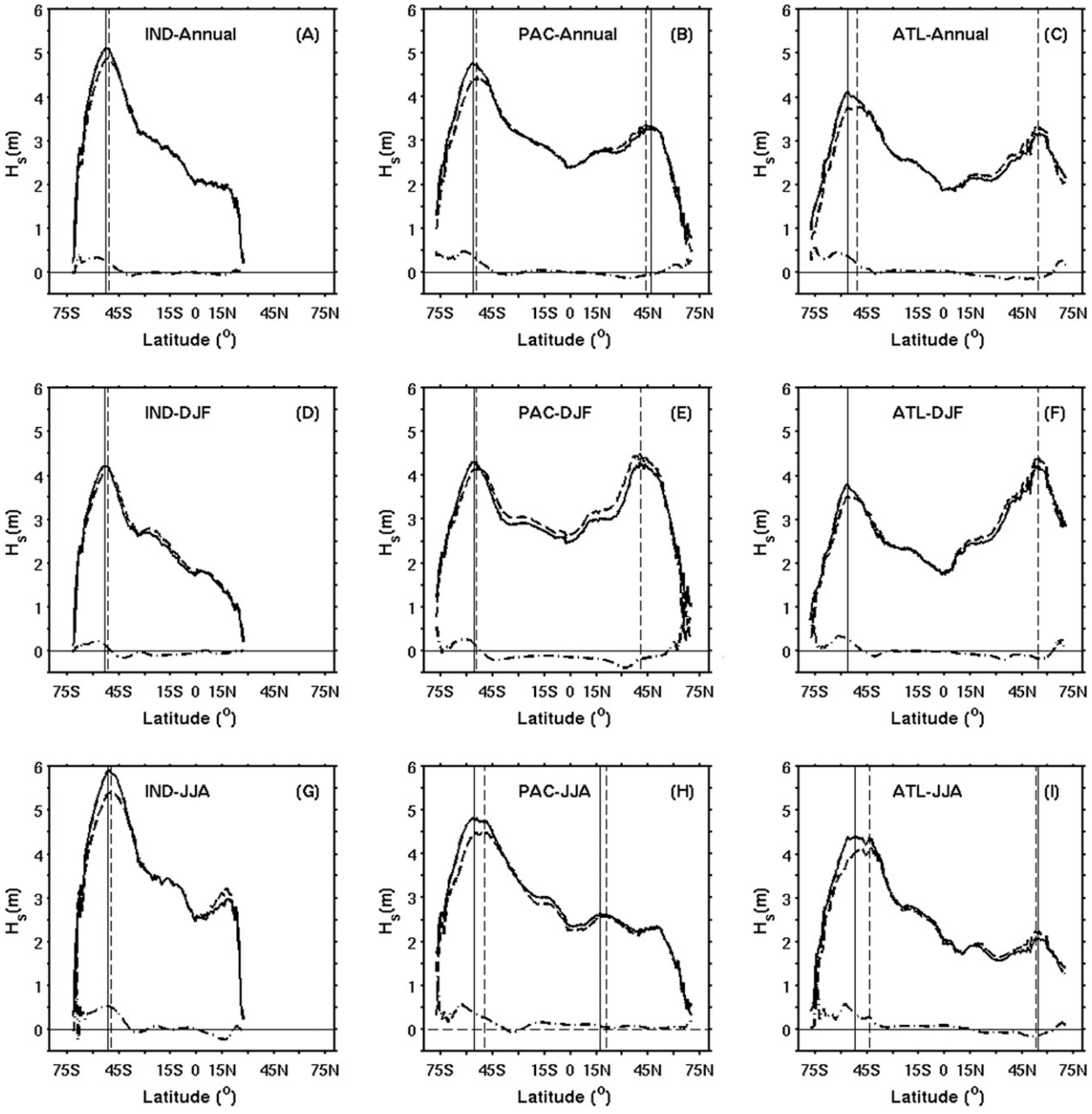

FIG. 9. Meridional cross sections of the zonally averaged annual, DJF, and JJA H_s (m) fields, for PC20 (dashed black line) and FC21 (black line), separated for each ocean basin: annual values in the (a) Indian, (b) Pacific, and (c) Atlantic Oceans; DJF values in the (d) Indian, (e) Pacific, and (f) Atlantic Oceans; and JJA values in the (g) Indian, (h) Pacific, and (i) Atlantic Oceans. The dotted–dashed line in all the panels represents the difference between FC21 and PC20. The vertical full (dashed) line represents the latitudinal position of the FC21 (PC20) Northern and Southern Hemispheres H_s (m) climatological mean maxima.

percentiles are computed globally for the latitude range of 70°S–70°N, and for the latitude bands in the middle to high latitudes, from 35°S/N to 70°S/N, in order to capture the wave heights variation in the extratropical storms areas. The axis range varies between the figure panels. The annual mean global percentiles (Fig. 10a) show a light but consistent increase of the FC21 wave heights. The DJF global percentiles (Fig. 9b), on the other hand, show a well-defined global decrease, while in JJA (Fig. 10c) a consistent increase in the global wave heights is to be expected. A consistent decrease in the annual and seasonal H_s percentiles of FC21, in the Northern Hemisphere middle to high latitudes is shown in Figs. 10d,e. To a certain extent the opposite can be seen in Figs. 10g–i for

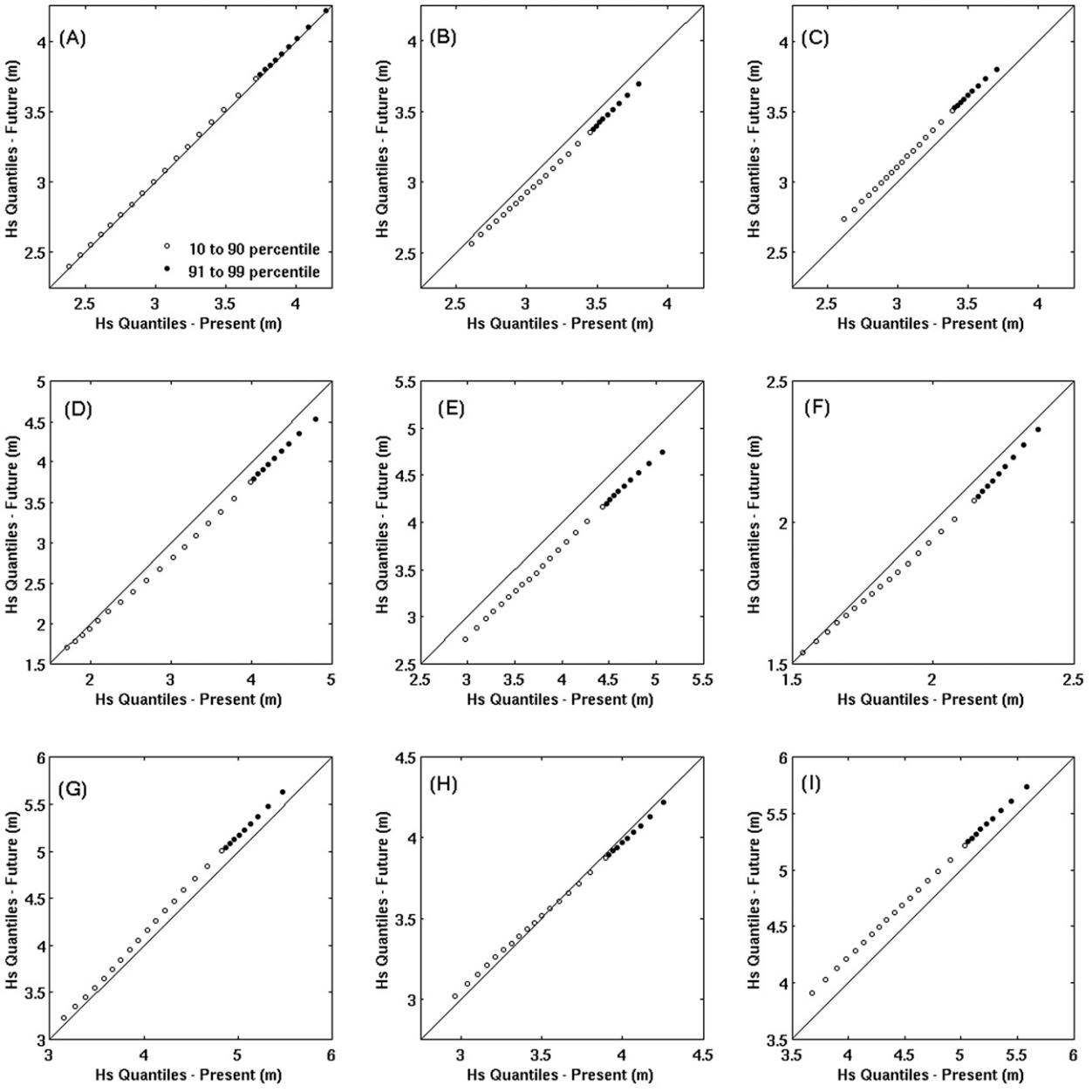

FIG. 10. Quantile–quantile comparisons of present and future (a),(d),(g) annual; (b),(e),(h) DJF; and (c),(f),(i) JJA H_s (m) global [(a)–(c) 70°S–70°N] and regional [(d)–(f) 35°–70°N and (g)–(i) 70°–35°S]. The legend in (a) applies to the all the panels.

the Southern Hemisphere, where the annual mean H_s percentiles (Fig. 10g) show an increase of the wave heights, particularly for the highest waves in the upper percentiles (90%–99%). In DJF (Fig. 10h) there is a slight increase in the wave heights shown in the lower percentiles of FC21 but a decrease in the extreme wave heights. In JJA (Fig. 10i), a consistent increase in all percentiles is found for the Southern Ocean storm belt.

The waves generated along the Southern Ocean storm belt have a considerable impact on the global wave climate due to swell propagation (Alves 2006). While the exact quantification of the relative weight of the Southern Ocean swell in the global wave climate remains an open issue, Sterl and Caires (2005) have demonstrated its importance on the variability of the global mean H_s. The increase of the projected future mean wave heights in the Southern Ocean and the south poleward shift of the climatological maxima, seen in the previous figures, can have an impact on the global mean wave periods, due to the increase of the wave heights at the generation area, on the one hand, and on the other hand due to a longer propagation distance to the equator.

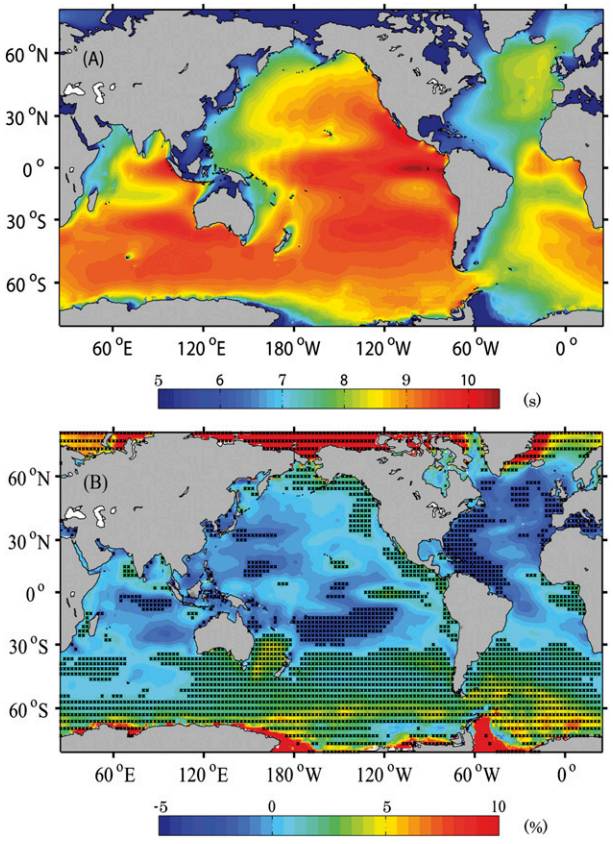

FIG. 11. As in Fig. 7, but for T_{m1} (s).

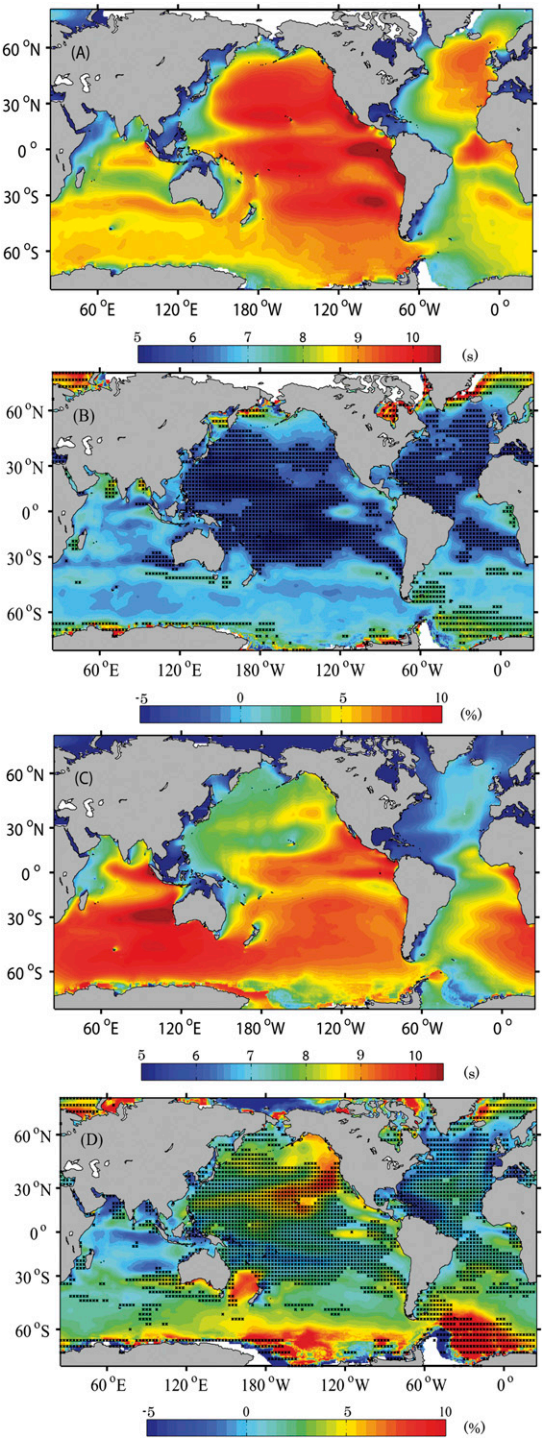

FIG. 12. As in Fig. 8, but for T_{m1} (s).

The impact of the projected changes in wave heights and the poleward displacement of the mean H_s climatological maxima (shown above) on the mean wave periods can be seen in Figs. 11 and 12. The present-day annual mean T_{m1}, and the normalized difference between future and present climates can be seen in Figs. 11a,b. The pattern of changes of the annual mean T_{m1} climate (Fig. 11b) shows large areas of statistically significant projected increase of the mean wave periods (higher than 5%), mostly in the Southern Hemisphere and in the Pacific Ocean, along the west coast of the American continent, but also in the east equatorial areas of the Indian and Atlantic Oceans (at the swell pools). In the higher latitudes of the Northern Hemisphere, in the Bering and Norwegian Seas, some increase of the annual mean T_{m1} (less than 5%) is also to be expected. The large projected increase of the annual mean T_{m1} values in the high latitudes, in the east coast of Greenland, in the Arctic Ocean, and close to Antarctica can be explained by ice retraction, as mentioned above for the H_s projections.

The projected changes in the DJF mean T_{m1} (Fig. 12b) show statistically significant decreases (2%–3% and about 5% in some areas) mostly in the Northern Hemisphere. Some increases are to be expected in the Atlantic sector of the Southern Ocean and in the swell pools (5% or less). On the contrary, the projected changes in the mean JJA T_{m1} (Fig. 12d) show a general increase in the future mean periods, with well-defined areas of statistically significant increases of mean periods in the Southern Hemisphere

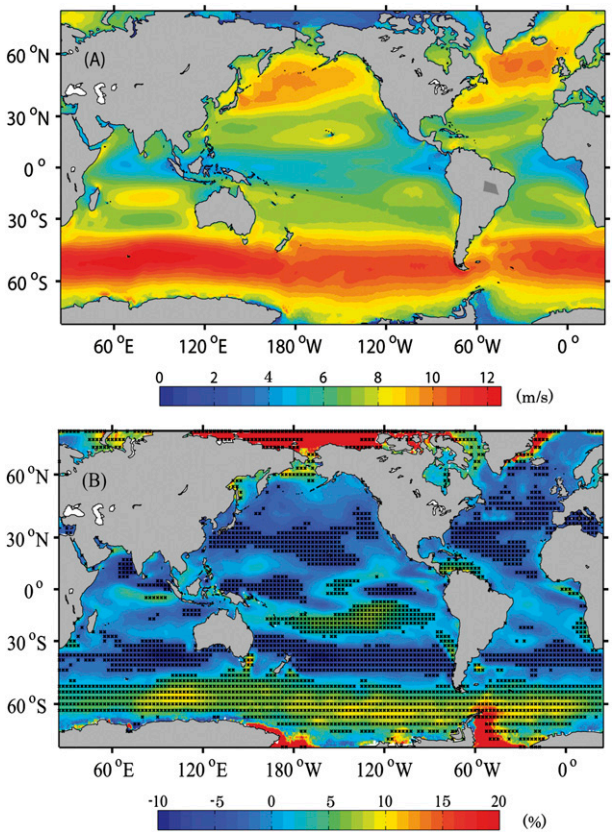

FIG. 13. As in Fig. 7, but for U_{10} ($m\,s^{-1}$).

(higher than 5% south of 30°S, reaching 10% in the high latitudes) and in the equatorial eastern side of the Pacific and Atlantic Oceans. It appears that the projected changes in the Southern Ocean wave heights in JJA shown above in Fig. 8d are responsible for the annual increase seen in Fig. 12d. As mentioned above, due to swell propagation, the connection between changes in the wind speed and changes in the ocean surface waves are not necessarily direct. Figures 13a,b shows the annual mean U_{10} from ECHAM5 for the present day and the normalized difference between future and present climates.

The projected changes in the annual mean U_{10} shown in Fig. 13b reveal statistically significant increases of the mean surface wind speed on the order of 10% or more (higher than $1\,m\,s^{-1}$) in the Southern Ocean Storm belt. The changes in the Southern Ocean are linked to the poleward shift of the annual climatological U_{10} maxima and to the increase of the wind speed at the maxima in the Indian, Pacific, and Atlantic sectors of the Southern Ocean (seen in Figs. 15a–c; as in Fig. 9 but for U_{10}). These changes do not have a correspondence in the midlatitudes of the Northern Hemisphere, where instead the annual mean U_{10} in the future will mostly decrease, with a poleward shift only noticeable in the North Pacific subbasin (Fig. 15b). The changes in the wind speed in the mid to high latitudes lead to the projected changes of the annual mean H_s seen in Figs. 7b and 9a–c. In the low latitudes the situation is more complex, and the projected increases in the annual mean U_{10} along the trade winds paths, statistically significant mostly in the Pacific Ocean (Figs. 13b, 15b), do not have a direct correspondence to the projected changes in the annual mean H_s there (see Figs. 7b, 9b).

In boreal winter the projected changes in the mean U_{10} (Figs. 14b, 15d–f) are, to a certain extent, similar to the annual projected changes: well-defined statistically significant increases in wind speed in the Southern Ocean and along the Southern Hemisphere trade winds and decreases in the North Pacific and North Atlantic. These changes are nevertheless more pronounced in the Southern Ocean, particularly in the South Pacific and South Atlantic trade winds path (Figs. 15e,f). A poleward shift of the climatological maxima is projected to occur in both hemispheres in DJF. In JJA the statistically significant projected changes in the mean U_{10} (Figs. 14d,c) are highest in an area south of Australia and New Zealand (15%–20%, corresponding to around $2\,m\,s^{-1}$), extending to the Tasman Sea, and along the Southern Hemisphere trade winds path, in the Indian, Pacific, and Atlantic Oceans. In the Northern Hemisphere, a decrease in the wind speed is projected to occur, mainly in the North Atlantic subbasin. These changes in the mean U_{10} during the austral winter can also be seen in Figs. 15g–i, where the projected poleward shift in the Southern Ocean but particularly the wind speed increase in the Indian Ocean Sector are clear. The projected decrease in the mean wind speed in the Northern Hemisphere midlatitudes in JJA, seen in Figs. 15g–i, show no significant shift in the position of the climatological maxima. The climatological wind speed maxima in the North Pacific subbasin is at the trade winds path (Fig. 15h), and an equatorward shift of this maxima, along with a decrease of the wind speed, is projected to occur.

5. Summary of results and conclusions

Changes in wave climate toward the end of the twenty-first century were analyzed from a global simulation with a dynamical wave model, driven by present-day and potential future atmospheric conditions under the IPCC A1B greenhouse gas emission scenario. The results of the comparisons and validation of the control run H_s, with reanalyses and buoy observations, respectively (Figs. 2–6), provided the necessary confidence in the wave model WAM ability to reproduce the global wave climate in the twenty-first century. These results follow from the quality of the ECHAM5 U_{10} winds, shown to have a good

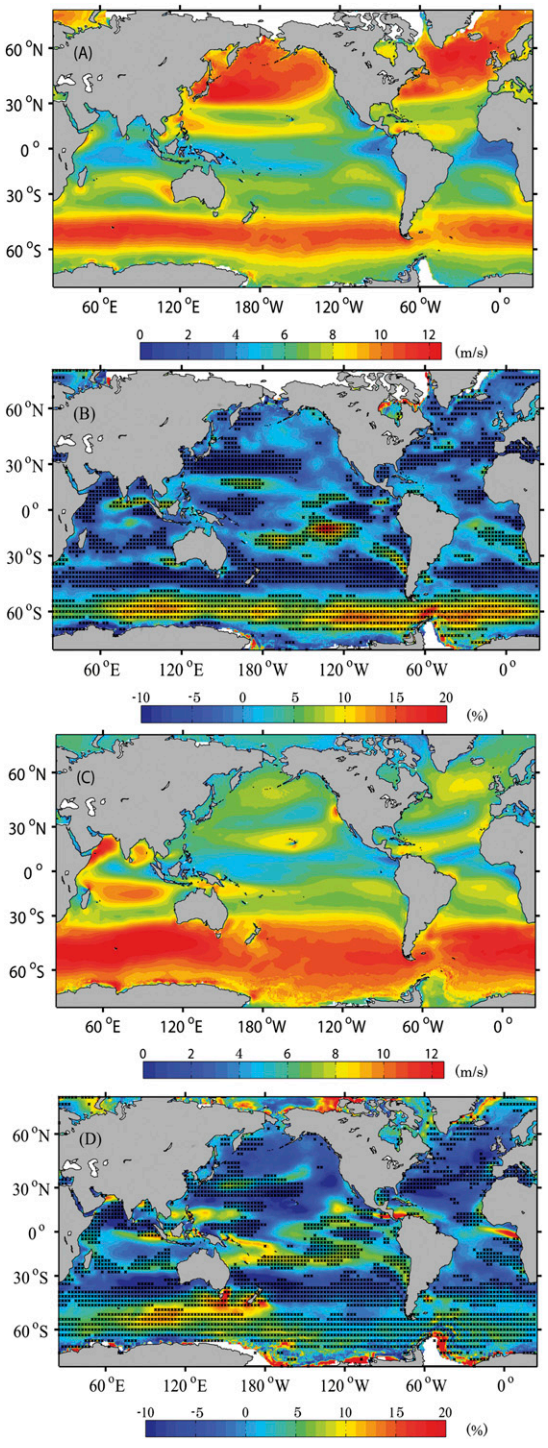

FIG. 14. As in Fig. 8, but for U_{10} (m s^{-1}).

agreement with the ERA-Interim reanalysis (Fig. 6), in line with what was shown by Bengtsson et al. (2009).

Because of global warming, the annual and seasonal mean H_s are projected to have increased and decreased over large areas of the global ocean by the end of the twenty-first century. At lower latitudes a decrease is predominant, while at higher latitudes, especially in the Southern Hemisphere, an increase is found (Figs. 7b, 9a–c). The projected increase in the annual global extreme wave heights has been shown to be very small (Fig. 10a). The seasonal projected future mean H_s revealed a general decrease of the wave heights in DJF (Figs. 8b, 9d–f), with the exception of the Southern Ocean, where an increase is to be expected, and a general increase in JJA (Figs. 8b, 9h,i), with the exception of the North Atlantic subbasin, where a moderate decrease of the wave heights was shown to be expected. The projected increase of the mean and extreme wave heights in the austral winter (Figs. 10c–i) was shown to be particularly intense along the Southern Ocean storm belt.

Figure 16 shows the time series of the globally averaged PC20 and FC21 yearly mean H_s. The yearly means are computed between 75°N to 75°S, and a latitudinal correction is applied (cosine of the latitude). The horizontal lines represent the global present-day and projected global mean wave heights for the respective 32-yr periods. The comparison between these means (2.08 m for PC20 and 2.13 m for FC21) shows an overall 5-cm (2.4%) projected increase of the global wave heights for the end of the twenty-first century. This increase is supported mainly by the ''all year round'' increase of the wave heights in the Southern Ocean storm belt, which is related to the projected changes in surface winds there. The projected changes in the mean and seasonal surface wind speeds are shown in Figs. 13–15: increase of the wind speeds and a poleward shift of the storm tracks, in line with the findings of Bengtsson et al. (2009).

As mentioned above, the connection between the climatological changes in the wind speeds and the changes in the wave heights is not necessarily direct because of the propagating effect of waves. This imbalance is a characteristic of the lower latitudes, where swell waves prevail. The comparison of the differences between the PC20 and FC21 meridional cross sections of wind speeds and wave heights (dotted–dashed lines in Figs. 9, 13) in the low latitudes shows than in some areas of the low latitudes the projected changes of the wind speed is of different sign of the ones for the wave heights: for example in the Pacific Ocean annual (Figs. 9b,e,h, 15b,e,h).

The projected changes in the wave heights shown here are consistent with those described in Mori et al. (2010), particularly in areas of increasing wave heights in the Southern Hemisphere. While also using wind fields from a GCM driven by the IPCC A1B emission scenario, the study of Mori et al. (2010) used data from a different atmospheric model and also utilized a different wave model (SWAN) and a lower resolution (1.25°) than the one used here. The results available from statistical

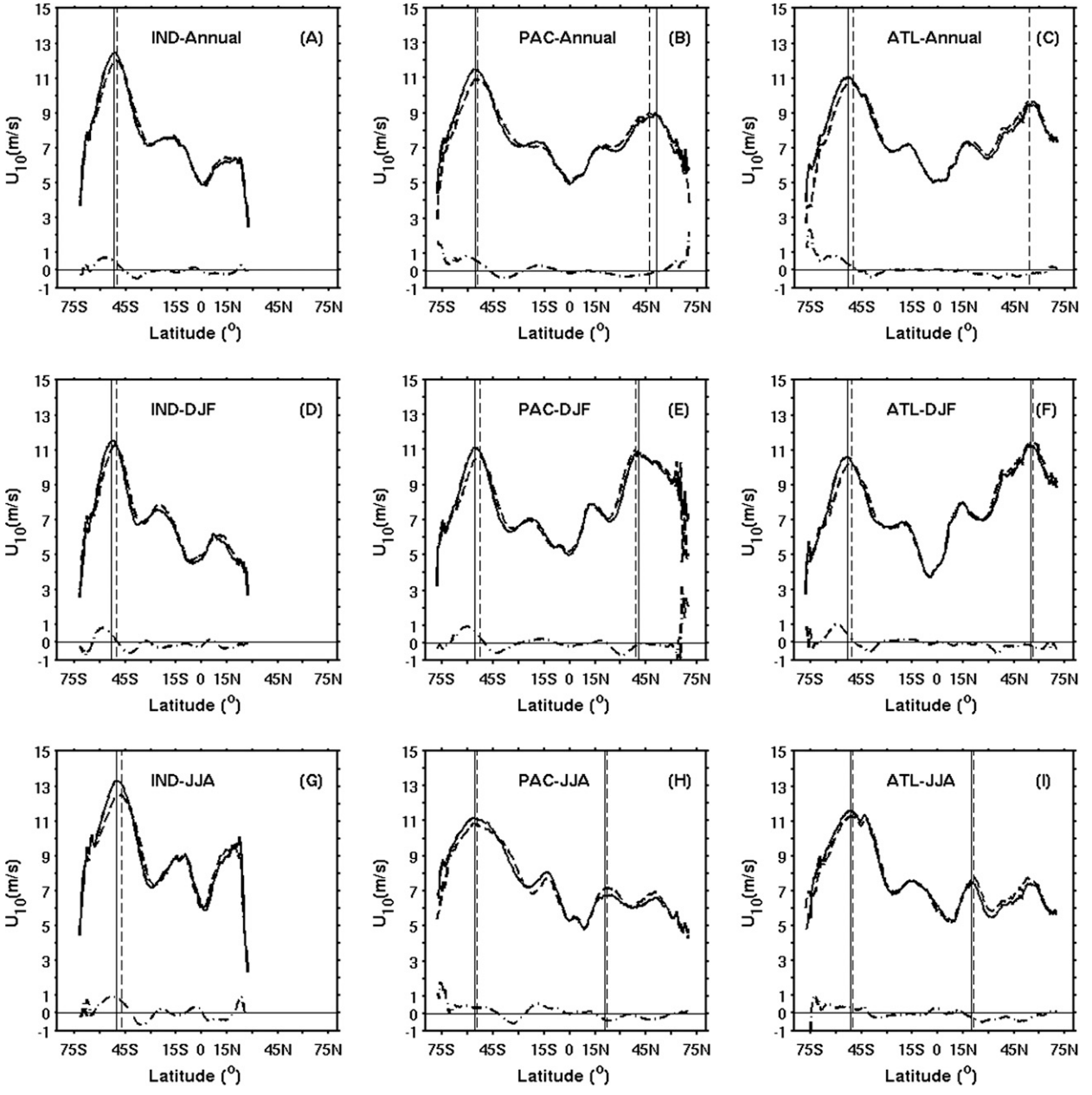

FIG. 15. As in Fig. 9, but for U_{10} (m s^{-1}).

approaches relating annual and seasonal means of significant wave height with sea level pressures, available for some more emission scenarios (e.g., Wang and Swail 2006a,b), point into a similar direction, namely a poleward shift of wave heights most likely associated with a poleward shift in midlatitude storm tracks.

The areas of projected changes in the annual T_{m1}, mostly in the tropics along the swell pools, are associated with the projected increase of wave heights in the Southern Ocean. The projected changes in the annual mean periods (Fig. 11a) show significant increases in the Southern Ocean storm belt and, due to swell propagation, in the eastern areas of the ocean basins, being more pronounced along the swell pools. These changes are more pronounced during the austral winter (Fig. 11c) and are associated with the strengthening of the Southern Ocean westerlies (Fig. 13) and with the poleward shift of the Southern Hemisphere extratropical storms.

The poleward shift in the wave activity in the middle and high latitudes of both hemispheres appears to be a consistent result emerging from this study. The shift is more pronounced in the Southern Hemisphere, where an

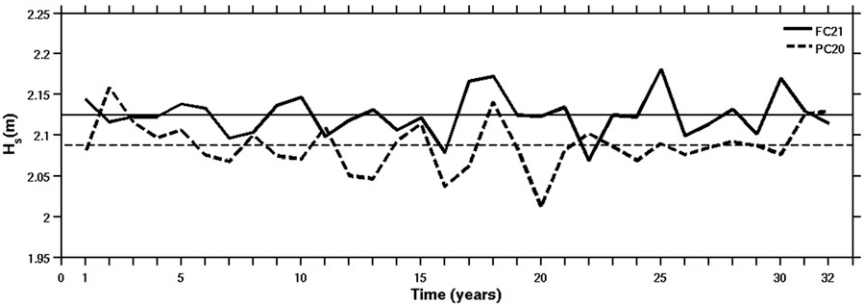

FIG. 16. Time series of the yearly mean globally averaged H_s (m) for PC20 (dashed line) and FC21 (full line). The horizontal full (dashed) line represents the global H_s (m) mean for the FC21 (PC20) period.

intensification of the westerlies also leads to an increase of the climatological wave maxima. We conclude that this is a robust feature most likely associated with corresponding shifts in the midlatitude storm tracks. The impact of this feature on the global and regional wave energy content should be addressed in future research. The impact of the changes induced by this feature in the swell domination in the global ocean should also be addressed in future research.

A larger ensemble of global wave climate projections using atmospheric forcing from different climate models using a range of emission scenarios is needed to fully assess the robustness of the features shown in this study and to provide a more comprehensive analyses of the uncertainties associated with different projections. This is the objective of the dynamically based global wave climate COWCLIP ensemble effort (Hemer et al. 2013), of which this study is part.

We have presented the fundamental features of projected changes in wave climate for the end of the twenty-first century based on H_s and T_{m1}. These two parameters offer only one perspective of the wave field characteristics, as two fields with the same and significant wave height and mean period may still be different in detail: a mixed sea state of wind sea and swell may have the same H_s and T_{m1} as a slightly higher wind sea without swell. To distinguish such conditions, additional information about the projected changes in the wind sea and swell significant wave heights and mean periods is needed. Detailed studies regarding the effects of projected intensification of tropical storms (Oouchi et al. 2006; Meehl et al. 2007; Bengtsson et al. 2007) in the global wave climate or the wave climate in a projected ice-free Artic Ocean are also needed.

Acknowledgments. The authors greatly appreciated the help of Noel Keenlyside, from the Leibniz Institute of Marine Sciences, in Germany, for his help preparing the ECHAM5 wind and ice fields, and the help of Jean Bidlot, from the ECMWF (Reading, United Kingdom) with the many details of the buoy data. The anonymous reviewers are thanked for their evaluation of this paper.

APPENDIX

Model Output Parameters and Buoy Details

Tables A1 and A2 show the integrated output parameters and the buoy details, respectively.

TABLE A1. Integrated output parameters.

Parameter No.	Parameter	Dimension
1	Wind speed U10	$m\,s^{-1}$
2	Wind direction	Degree from north (toward)
3	Friction velocity	$m\,s^{-1}$
4	Drag coefficient	
5	Water depth	m
6	Current speed	$m\,s^{-1}$
7	Current direction	Degree from north (toward)
8	Significant wave height	m
9	Wave peak period	s
10	Wave mean period	s
11	Wave T_{m1} period	s
12	Wave T_{m2} period	s
13	Wave direction	Degree from north (toward)
14	Directional spread	Degree
15	Normalized wave stress	%
16	Sea significant wave height	m
17	Sea peak period	s
18	Sea mean period	s
19	Sea T_{m1} period	s
20	Sea T_{m2} period	s
21	Sea direction	Degree from north (toward)
22	Sea directional spread	Degree
23	Swell significant wave height	m
24	Swell peak period	s
25	Swell mean period	s
26	Swell T_{m1} period	s
27	Swell T_{m2} period	s
28	Swell direction	Degree from north (toward)
29	Swell directional spread	Degree

TABLE A2. Buoy details.

No.	WMO ID	Position	Period (years)	No.	WMO ID	Position	Period (years)
1	26874	40°15′02″N 73°10′12″W	19	28	46001	56°18′16″N 147°55′13″W	10
2	63108	60°48′05″N 1°42′01″E	19	29	62091	53°28′08″N 5°25′05″W	10
3	62103	49°54′00″N 2°54′00″W	17	30	42001	25°53′16″N 89°39′27″W	10
4	44009	38°27′49″N 74°42′07″W	16	31	46012	37°21′45″N 122°52′52″W	10
5	16415	48°28′12″N 126°00′06″W	12	32	62132	56°24′02″N 2°00′05″E	10
6	46042	36°47′07″N 122°28′09″W	15	33	62081	51°00′00″N 13°18′04″W	10
7	44025	40°15′00″N 73°10′00″W	13	34	62112	58°42′02″N 1°18′00″E	10
8	21199	49°30′00″N 69°25′00″W	13	35	11543	15°54′02″N 57°54′04″W	10
9	16306	43°24′05″N 7°48′01″E	13	36	11529	28°30′36″N 84°30′36″W	10
10	62107	50°6′9″N 6°06′00″W	12	37	11193	38°12′00″N 123°18′01″W	10
11	42035	29°13′54″N 94°24′46″W	12	38	11151	42°06′02″N 4°42′01″E	10
12	63103	61°12′00″N 1°06′01″E	12	39	11040	57°01′02″N 0°00′03″E	10
13	62133	57°06′05″N 1°00′01″E	12	40	10939	64°06′00″N 22°54′01″W	10
14	16072	28°30′00″N 80°10′06″W	12	41	10876	28°06′02″N 126°18′03″E	10
15	46047	32°24′11″N 119°32′8″W	12	42	10823	42°42′01″N 68°18′03″W	10
16	41004	32°30′2″N 79°5′58″W	12	43	10721	23°24′02″N 162°16′12″W	10
17	62145	53°06′9″N 2°48′00″E	12	44	10630	41°04′48″N 66°34′46″W	10
18	42002	25°47′24″N 93°39′58″W	12	45	10576	51°51′01″N 155°55′12″W	10
19	44014	36°36′41″N 74°50′31″W	12	46	10505	59°30′02″N 1°30′03″E	10
20	42001	25°53′16″N 89°39′27″W	12	47	10482	23°24′01″N 162°10′00″W	10
21	62029	48°42′02″N 12°24′02″W	11	48	10467	37°21′36″N 122°52′48″W	10
22	46005	46°5′59″N 131°0′5″W	11	49	10334	37°58′48″N 130°00′02″W	10
23	42003	26°02′38″N 85°36′42″W	11	50	10165	65°42′02″N 24°48′08″W	10
24	46001	56°18′16″N 147°55′13″W	10	51	10157	25°53′24″N 93°34′12″W	10
25	62023	51°24′00″N 7°55′00″W	10	52	10110	43°30′04″N 67°54′02″W	10
26	62142	53°00′00″N 2°06′05″E	10	53	11727	18°00′04″S 85°06′02″W	9
27	62001	45°12′2″N 5°00′05″W	10	54	33620	0°00′00″ 153°54′02″W	8

REFERENCES

Alves, J. H. G. M., 2006: Numerical modeling of ocean swell contributions to the global wind-wave climate. *Ocean Modell.,* **11,** 98–122.

Bengtsson, L., K. Hodges, and E. Roeckner, 2006: Storm tracks and climate change. *J. Climate,* **19,** 3518–3543.

——, ——, M. Esch, N. Keenlyside, L. Kornblueh, J.-J. Luo, and T. Yamagata, 2007: How may tropical cyclones change in a warmer climate? *Tellus,* **59A,** 539–561.

——, ——, and N. Keenlyside, 2009: Will extratropical storms intensify in a warmer climate? *J. Climate,* **22,** 2276–2301.

Bidlot, J.-R., 2001: ECMWF wave model products. *ECMWF Newsletter,* No. 91, ECMWF, Reading, United Kingdom, 9–15.

——, 2012: Present status of wave forecasting at ECMWF. *Proc. Workshop on Ocean Waves,* Reading, United Kingdom, ECMWF, 1–15.

——, D. J. Holmes, P. A. Wittmann, R. Lalbeharry, and H. S. Chen, 2002: Intercomparison of the performance of operational ocean wave forecasting systems with buoy data. *Wea. Forecasting,* **17,** 287–310.

——, P. Janssen, and S. Abdalla, 2007: A revised formulation of ocean wave dissipation and its model impact. ECMWF Tech. Memo. 509, ECMWF, Reading, United Kingdom, 27 pp. [Available online at http://www.ecmwf.int/publications/.]

Booij, N., R. C. Ris, and L. H. Holthuijsen, 1999: A third generation wave model for coastal regions: 1. Model description and validation. *J. Geophys. Res.,* **104** (C4), 7649–7666.

Caires, S., and A. Sterl, 2005: 100-year return value estimates for ocean wind speed and significant wave height from the ERA-40 data. *J. Climate,* **18,** 1032–1048.

——, ——, J.-R. Bidlot, N. Graham, and V. Swail, 2004: Intercomparison of different wind wave reanalyses. *J. Climate,* **17,** 1893–1913.

——, ——, and C. P. Gommenginger, 2005: Global ocean mean wave period data: Validation and description. *J. Geophys. Res.,* **110,** C02003, doi:10.1029/2004JC002631.

Cavaleri, L., B. Fox-Kemper, and M. Hemer, 2012: Wind waves in the coupled climate system. *Bull. Amer. Meteor. Soc.,* **93,** 1651–1661.

Chawla, A., D. Spindler, and H. L. Tolman, 2011: A thirty year wave hindcast using the latest NCEP Climate Forecast System Reanalysis winds. *Proc. 12th Int. Workshop on Wave Hindcasting and Forecasting,* Waikoloa, HI, Environment Canada, I1.

——, ——, and ——, 2013: Validation of a thirty year wave hindcast using the Climate Forecast System Reanalysis winds. *Ocean Modell.,* **70,** 189–206.

Chen, G., B. Chapron, R. Ezraty, and D. Vandemark, 2002: A global view of swell and wind sea climate in the ocean by satellite altimeter and scatterometer. *J. Atmos. Oceanic Technol.,* **19,** 1849–1859.

Debernhard, J., and L. Roed, 2008: Future wind, wave and storm surge climate in the Northern Seas: A revisit. *Tellus,* **60A,** 427–438, doi:10.1111/j.1600-0870.2008.00312.x.

——, Ø. Sætra, and L. Roed, 2002: Future wind, wave and storm surge climate in the northern seas. *Climate Res.,* **23,** 39–49.

Dee, D. P., and S. Uppala, 2009: Variational bias correction of satellite radiance data in the ERA-Interim reanalysis. *Quart. J. Roy. Meteor. Soc.,* **135,** 1830–1841.

——, and Coauthors, 2011: The ERA-Interim reanalysis: Configuration and performance of the data assimilation system. *Quart. J. Roy. Meteor. Soc.,* **137,** 553–597.

Grabemann, I., and R. Weisse, 2008: Climate change impact on extreme wave conditions in the North Sea: An ensemble study. *Ocean Dyn.,* **58,** 199–212, doi:10.1007/s10236-008-0141-x.

Gulev, S. K., and V. Grigorieva, 2004: Last century changes in ocean wind wave height from global visual wave data. *Geophys. Res. Lett.,* **31,** L24302, doi:10.1029/2004GL021040.

——, ——, A. Sterl, and D. Woolf, 2003: Assessment of the reliability of wave observations from voluntary observing ships: Insights from the validation of a global wind wave climatology based on voluntary observing ship data. *J. Geophys. Res.,* **108,** 3236, doi:10.1029/2002JC001437.

Günther, H., S. Hasselmann, and P. A. E. M. Janssen, 1992: The WAM model cycle 4.0, user manual. Deutsches Klimarechenzentrum Tech. Rep. 4, 102 pp.

Hanley, K. E., S. E. Belcher, and P. P. Sullivan, 2010: A global climatology of wind–wave interaction. *J. Phys. Oceanogr.,* **40,** 1263–1282.

Hemer, M., X. L. Wang, R. Weisse, and V. R. Swail, 2012: Advancing wind-waves climate science: The COWCLIP project. *Bull. Amer. Meteor. Soc.,* **93,** 791–796.

——, Y. Fan, N. Mori, A. Semedo, and X. Wang, 2013: Projected changes in wave climate from a multi-model ensemble. *Nat. Climate Change,* **3,** 471–476, doi:10.1038/NCLIMATE1791.

Hersbach, H., and P. A. E. M. Janssen, 1999: Improvements of the short fetch behavior in the WAM model. *J. Atmos. Oceanic Technol.,* **16,** 884–892.

Högström, U., A. Smedman, E. Sahlée, W. M. Drennan, K. K. Kahma, C. Johansson, H. Pettersson, and F. Zhang, 2009: The atmospheric boundary layer during swell: A field study and interpretation of the turbulent kinetic energy budget for high wave ages. *J. Atmos. Sci.,* **66,** 2764–2779.

Janssen, P. A. E. M., 1991: Quasi-linear theory of wind wave generation applied to wave forecasting. *J. Phys. Oceanogr.,* **21,** 1631–1642.

——, 2004: *The Interaction of Ocean Waves and Wind.* Cambridge University Press, 300 pp.

Kaas, E., and Coauthors, 2001: STOWASUS 2100: Regional storm, wave and surge scenarios for the 2100 century. Final Rep. ENV4-CT97-04989. Danish Meteorological Institute Final Rep. ENV4-CT97-04989, 134 pp. [Available online at http://web.dmi.dk/pub/STOWASUS-2100/Final/Final.pdf.]

Kitoh, A., and Coauthors, 2009: Projection of changes in future weather extremes using super-high-resolution global and regional atmospheric models in the KAKUSHIN program: Results of preliminary experiments. *Hydrol. Res. Lett.,* **3,** 49–53, doi:10.3178/hrl.3.49.

Komen, G. J., L. Cavaleri, M. Donelan, K. Hasselmann, S. Hasselmann, and P. A. E. M. Janssen, 1994: *Dynamics and Modelling of Ocean Waves.* Cambridge University Press, 560 pp.

Lowe, J. A., and Coauthors, 2009: UK climate projections science report: Marine and coastal projections. Met Office Hadley Centre Rep., 12 pp.

Meehl, G. A., and Coauthors, 2007: Global climate projections. *Climate Change 2007: The Physical Science Basis,* S. Solomon et al., Eds., Cambridge University Press, 747–845.

Mori, N., T. Yasuda, H. Mase, T. Tom, and Y. Oku, 2010: Projections of extreme wave climate change under global warming. *Hyrol. Res. Lett.,* **4,** 15–19.

NGDC, cited 2010: ETOPO1 Global Relief Model. [Available online at http://www.ngdc.noaa.gov/mgg/global/global.html.]

Nilsson, E. O., A. Rutgersson, A.-S. Smedman, and P. P. Sullivan, 2012: Convective boundary layer structure in the presence of wind-following swell. *Quart. J. Roy. Meteor. Soc.,* **138,** 1476–1489.

Oouchi, K., J. Yoshimura, H. Yoshimura, R. Mizuta, S. Kusunoki, and A. Noda, 2006: Tropical cyclone climatology in a global warming climate as simulated in a 20 km-mesh global atmospheric model: Frequency and wind intensity analysis. *J. Meteor. Soc. Japan,* **84,** 259–276.

Roeckner, E., and Coauthors, 2003: The atmospheric general circulation model ECHAM 5. Part I: Model description. Max Planck Institute for Meteorology Rep. 349, 140 pp.

Semedo, A., Ø. Sætra, A. Rutgersson, K. K. Kahma, and H. Pettersson, 2009: Wave-induced wind in the marine boundary layer. *J. Atmos. Sci.,* **66,** 2256–2271.

——, K. Sušelj, A. Rutgersson, and A. Sterl, 2011: A global view on the wind sea and swell climate and variability from ERA-40. *J. Climate,* **24,** 1461–1479.

Smedman, A.-S., U. Högström, E. Sahleé, W. M. Drennan, K. K. Kahma, H. Pettersson, and F. Zhang, 2009: Observational study of marine atmospheric boundary layer characteristics during swell. *J. Atmos. Sci.,* **66,** 2747–2763.

Solomon, S., D. Qin, M. Manning, Z. Chen, M. Marquis, K. Averyt, M. Tignor, and H. L. Miller Jr., Eds., 2007: *Climate Change 2007: The Physical Science Basis.* Cambridge University Press, 996 pp.

Sterl, A., and S. Caires, 2005: Climatology, variability and extrema of ocean waves: The web-based KNMI/ERA-40 wave atlas. *Int. J. Climatol.,* **25,** 963–977.

Sullivan, P. P., J. B. Edson, T. Hristov, and J. C. McWilliams, 2008: Large eddy simulations and observations of atmospheric marine boundary layers above nonequilibrium surface waves. *J. Atmos. Sci.,* **65,** 1225–1245.

Uppala, S. M., and Coauthors, 2005: The ERA-40 Re-Analysis. *Quart. J. Roy. Meteor. Soc.,* **131,** 2961–3012.

WAMDI Group, 1988: The WAM model—A third generation ocean wave prediction model *J. Phys. Oceanogr.,* **18,** 1775–1810.

Wang, X., and V. Swail, 2006a: Historical and possible future changes of wave heights in Northern Hemisphere oceans. *Atmosphere Ocean Interactions,* Vol. 2, W. A. Perrie, Ed., WIT Press, 185–219.

——, and ——, 2006b: Climate change signal and uncertainty in projections of ocean wave heights. *Climate Dyn.,* **26,** 109–126, doi:10.1007/s00382-005-0080-x.

——, F. Zwiers, and V. Swail, 2004: North Atlantic Ocean wave climate change scenarios for the twenty-first century. *J. Climate,* **17,** 2368–2383.

WASA Group, 1998: Changing waves and storms in the northeast Atlantic? *Bull. Amer. Meteor. Soc.,* **79,** 741–760.

Young, I. R., 1999: Seasonal variability of the global ocean wind and wave climate. *Int. J. Climatol.,* **19,** 931–950.

——, S. Zieger, and V. Babanin, 2011: Global trends in wind speed and wave height. *Science,* **332,** 451–455.

Zacharioudaki, A., S. Pan, D. Simmonds, V. Magar, and D. E. Reeve, 2011: Future wave climate over the west-European shelf seas. *Ocean Dyn.,* **61,** 807–827.